International Journal of Thermophysics, Vol. 20, No. 2, 1999

Thermophysical Properties of Gaseous CF_4 and C_2F_6 from Speed-of-Sound Measurements

J. J. Hurly[1]

Received November 5, 1998

A cylindrical resonator was employed to measure the sound speeds in gaseous CF_4 and C_2F_6. The CF_4 measurements span the temperature range 300 to 475 K, while the C_2F_6 measurements range from 210 to 475 K. For both gases, the pressure range was 0.1 MPa to the lesser of 1.5 MPa or 80% of the sample's vapor pressure. Typically, the speeds of sound have a relative uncertainty of less than 0.01% and the ideal-gas heat capacities derived from them have a relative uncertainty of less than 0.1%. The heat capacities agree with those determined from spectroscopic data. The sound speeds were fitted with the virial equation of state to obtain the temperature-dependent density virial coefficients. Two models for the virial coefficients were employed, one based on square-well potentials and the second based on a Kihara spherical-core potential. The resulting virial equations reproduce the sound-speed measurements to within 0.005% and yield densities with relative uncertainties of 0.1% or less. The viscosity calculated from the Kihara potential is 2 to 11% less than the measured viscosity.

KEY WORDS: CF_4; C_2F_6; equation of state; hexafluoroethane; speed of sound; tetrafluoromethane; thermodynamic properties; virial coefficients.

1. INTRODUCTION

The thermophysical properties of the gases used by the semiconductor processing industry are needed for process modeling and for the accurate calibration of mass flow controllers (MFCs). The actual calibration of the MFCs is performed with nonhazardous surrogate gases such as tetrafluoromethane (CF_4) and hexafluoroethane (C_2F_6), whose thermophysical properties are also required. Prior to handling hazardous process gases, we

[1] Physical and Chemical Properties Division, Chemical Science and Technology Laboratory, National Institute of Standards and Technology, Gaithersburg, Maryland 20899, U.S.A.

0195-928X/99/0300-0455$16.00/0

chose to study the surrogate gases CF_4 and C_2F_6, and below, we report the results obtained.

Our laboratory has developed a highly precise, automated apparatus for measuring sound speeds in hazardous and/or corrosive process gases throughout the temperature and pressure ranges of interest for semiconductor processing ($200 \leqslant T \leqslant 480$ K and $P \leqslant 1.5$ MPa). The analysis of measured sound speeds provides the ideal-gas heat capacities $C_p^0(T)$ and the nonidealities of these gases.

The speed of sound, $u(P, T)$, measurements for CF_4 span the temperature range 300 K $\leqslant T \leqslant$ 475 K and pressures below the lesser of 1.5 MPa or 80% of the sample's vapor pressure. Highly precise sound speeds in CF_4 were reported by Ewing and Trusler [1] in the ranges 175 K $\leqslant T \leqslant$ 300 K and $P < 1.0$ MPa or 80% of the vapor pressure. Ewing and Trusler data were included when we fit the present data. Measurements of $u(T, P)$ in C_2F_6 cover the ranges 210 K $\leqslant T \leqslant$ 475 K and the lesser of $P < 1.5$ MPa or 80% of the vapor pressure.

The sound-speed measurements were collected along isotherms whose zero-pressure intercepts provided $C_p^0(T)$. The density virial coefficients that appear in the virial equation of state,

$$P = RT\rho[1 + B(T)\,\rho + C(T)\,\rho^2 + D(T)\,\rho^3 + \cdots] \tag{1}$$

were obtained by fitting the $u(T, P)$ data, where P is the pressure, T is the temperature, ρ is the density, and R is the gas constant. The virial expansion was truncated after the second and third density virial coefficients, $B(T)$ and $C(T)$, for CF_4 and after $D(T)$ for C_2F_6. Two methods were employed for determining $B(T)$ and $C(T)$ for each gas. The first method used the exact algebraic expressions for $B(T)$ and $C(T)$ derived from the hard-core square-well (HCSW) intermolecular potential model. Six parameters were required because different square-well parameters were used for $B(T)$ and $C(T)$. The second method used numerical representations of $B(T)$ and $C(T)$ obtained from a numerical integration over a Kihara spherical core [2] with the inclusion of three-body effects in $C(T)$. The Kihara model is often referred to as the hard-core Lennard–Jones (HCLJ) potential model. The HCLJ model uses only four parameters, but it requires more computation to generate and use than the HCSW model. The fourth virial coefficient $D(T)$ for C_2F_6 was described by a two-term inverse T polynomial.

In most cases, the values of $B(T)$ determined from the fit to the sound-speed measurements agree with previously published values within their combined uncertainties. For CF_4, the present measurements greatly reduce the uncertainty of $B(T)$. The values of $C(T)$ for CF_4 reported here agree

with the limited values previously available. For C_2F_6, few previous measurements of $B(T)$ have been reported, and no measurements of $C(T)$ were found in the literature.

The virial equations of state presented here for each fluid reproduce nearly all the $u(P, T)$ data to within $\pm 0.005\%$ of u. The virial equations are expected to generate vapor densities and ideal-gas heat capacities with uncertainties of less than 0.1% throughout the experimental temperature and pressure ranges, and they can be extrapolated to higher temperatures. The virial coefficients and transport properties calculated from the deduced HCLJ potential show a predictive ability over the wide temperature range where the two-body approximation is appropriate.

2. APPARATUS

The apparatus employed here was adapted from that used for the successful study of more than 20 nonhazardous gases and gas mixtures [3, 4]. The precursor apparatus and the acoustic model have been described in detail elsewhere [5, 6]. For the current work, the previous apparatus was modified to handle the hazardous, reactive, and corrosive gases employed in the semiconductor processing industry. These modifications address the reactive nature of the gases and their safe handling and disposal.

The entire apparatus is automated. All valves are air-operated from a remote control panel and/or computer. The entire system is enclosed in a walk-in gas cabinet which conforms to Article 51 of the Uniform Fire Code for Semiconductor Fabrication Facilities [7]. The cabinet encloses the acoustic resonator, gas manifold, pressure controller, temperature bath, pumps, sample bottles, and transducers. The cabinet provides secondary containment of the process gases, protecting personnel from a catastrophic failure. Passive and active interlocks are employed to prevent overpressure or overheating. The system has a maximum allowable working pressure of 1.5 MPa, the full-scale reading of our pressure controller. All surfaces in contact with the sample gas are constructed of corrosion resistant alloys. Where practical, ASME [8]-certified welds are used for joints. Welds were internally borescoped to assure full penetration. Welding was performed in a class 100 clean room, using a high-purity purge gas filtered to 0.02 μm, where moisture and oxygen levels were less than 1 ppm. Nickel gasket connections are utilized wherever mechanical connections are required. Where possible, the apparatus incorporates commercially available vacuum pumps, pump oil, valves, and transducers that have been specifically designed for semiconductor processing service.

A brief description of the experimental setup follows. The heart of the apparatus was an acoustic resonator (Fig. 1). The resonator was a

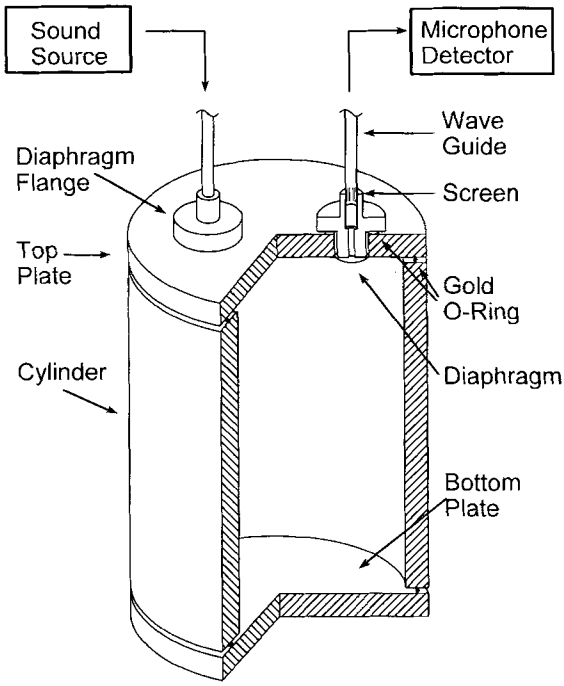

Fig. 1. Schematic of cylindrical acoustic resonator.

14-cm-long cylindrical cavity that had been bored out of an Alloy 400 ($\sim$67% Ni, $\sim$33% Cu) cylinder. The cavity had an inner diameter of 6.5 cm and an outer diameter of 7.8 cm. Circular Alloy 400 plates (1.3 cm thick) were bolted to the ends of the cavity and sealed with gold O-rings. One end plate contained two thin metal diaphragms mounted flush with the interior surface of the cavity. These diaphragms isolated the sample gas while coupling acoustic energy into and out of the cavity. The diaphragms were Alloy 400 disks (1 cm in diameter, 25 μm thick) that had been electron beam welded around their circumferences to small flanges mounted on the top end plate. Acoustic wave guides led from each diaphragm to remote electroacoustic transducers at ambient temperature. When sample gas was present in the cavity, a pressure controller maintained an equal pressure of argon in the wave guides. Thus, the thin metal diaphragms were not stretched by a differential pressure. The wave guides were commercially purchased horn-shaped tubes with a length of 15 cm and a diameter that tapers exponentially from 0.12 to 0.33 cm. A 2.5-cm-long, thin-walled stainless-steel tube connected the horns to gas-tight transducer housings that were also maintained at the sample pressure with argon. In the narrow

end of each horn, the manufacturer had installed a metal screen which damped resonances within the wave guide. When the wave guides were filled with argon, the horns strongly attenuated sound at frequencies above 8 kHz, setting an upper limit to the frequencies which could be studied.

The sound generator was a commercially manufactured earphone speaker. The sound was transmitted down a wave guide through one metal diaphragm into the resonator. The acoustic energy within the resonator was then coupled through the second metal diaphragm up the second wave guide to the sound detector, which was a commercially manufactured microphone designed as a hearing aid. Typically the frequency of the generator was scanned through two longitudinal modes [(3, 0, 0), (4, 0, 0)] and one radial mode [(0, 0, 1)]. The modes are labeled with the notation (K, N, S) of Gillis [5]. The frequency, f_{KNS}, and the half-width, g_{KNS}, of each resonance were measured using standard procedures [5] and instruments. Typically, the standard deviation of f_{KNS} was less than $10^{-5} f_{KNS}$. The speeds of sound and their uncertainties were computed from weighted averages of the results for the three modes. The relative uncertainties of u ranged from $(10 \text{ to } 100) \times 10^{-6}$, varying roughly as P^{-2}.

The resonator was suspended vertically in a well-stirred thermostated bath of either silicon oil or methanol. The bath was controlled within 2 mK of each set point by a proportional controller that used the output of a resistance bridge incorporating a thermistor. The temperature of the resonator was determined with a 25-Ω capsule-type standard platinum resistance thermometer (SPRT) that had been calibrated on ITS-90 and embedded in an aluminum block fastened to the resonator. Four-wire resistance measurements of the SPRT were made with a suitable DC multimeter.

A 13-kPa full-scale capacitance differential pressure transducer (DPT) was used to detect the differential pressure between the argon and the sample gas. The DPT was calibrated for pressure and temperature dependences and thermostated with a stability of ± 0.1 K. Pressure measurements were made on the argon side of the DPT with a quartz-Bourdon-tube differential pressure gauge. The reference side of the gauge was maintained below 2 Pa with a rotary pump. This Bourdon-tube gauge had been calibrated with a deadweight gauge and had a standard uncertainty in pressure of $\sigma_P = 30 \text{ Pa} + 0.0001 \times P$.

3. PROCEDURES

Measurements were made along isotherms by loading the resonator initially to the lesser of 1.5 MPa or 80% of the sample's vapor pressure. The temperature and pressure were allowed to equilibrate, and the frequencies and widths of the acoustic resonances were measured. The temperature

was maintained, and the pressure was reduced in successive steps. For each step, the air-operated valves were opened briefly and a portion of the sample gas was collected in a vessel cooled with liquid nitrogen. Once the pressure was reduced, the apparatus was allowed to return to equilibrium and the frequencies and widths were measured at the new state point.

The temperature-dependent effective radius, $a(T)$, and length, $l(T)$, of the cylindrical resonator were required to determine the sound speed from the resonance frequencies. These dimensions were determined as functions of the temperature by measuring the resonance frequencies when the resonator was filled with argon, a gas for which the speed of sound is accurately known. Because the calibration and the final measurements were conducted in the same thermal environment, there was a high degree of compensation for the effects of temperature gradients in the bath and even for systematic uncertainties in the measurement of temperature.

At each state point, the drive frequency was stepped through the resonance and amplitudes of the signal from the detector were recorded. Measurements were made at 11 frequencies spanning $f_{KNS} \pm g_{KNS}$ for each mode (K, N, S). A theoretically expected six-or eighth-parameter function was then fit to the amplitudes measured at each frequency, providing both f_{KNS} and g_{KNS}.

For a cylindrical cavity with a radius a and length l, discrete values of the wave number k_{KNS} are known [9]. The sound speed u in the sample gas is determined by dividing the measured f_{KNS} by $k_{KNS}/2\pi$. The measured resonance frequencies were corrected [5, 6] for the thermal and viscous losses at the boundaries and for the small effects of the tube used to move sample into and out of the cavity.

4. RESULTS

At each temperature and pressure, two longitudinal and one radial modes were used to compute values of the speed of sound. The mean of these three values and their relative standard deviation $\sigma[u]/u \times 10^6$ are tabulated in the Appendix (Table AI for CF_4 and Table AII for C_2F_6). The CF_4 measurements span the temperature range 300 to 475 K, while the C_2F_6 measurements range from 210 to 475 K. In both cases, the pressure range examined was 0.1 to the lesser of 1.5 MPa or 80% of the sample's vapor pressure.

The sound-speed measurements were taken along isotherms. The data on each isotherm were fitted to the acoustical virial equation of state:

$$u^2 = \frac{\gamma^0 RT}{m}\left(1 + \frac{\beta_a p}{RT} + \frac{\gamma_a p^2}{RT} + \frac{\delta_a p^3}{RT} + \cdots\right) \tag{2}$$

Table I. Ideal-Gas Heat Capacities, $C_p^0(T)$, Determined from each Isotherm

CF_4		C_2F_6			
T(K)	$C_p^0(T)/R$	T(K)	$C_p^0(T)/R$	T(K)	$C_p^0(T)/R$
300.0	7.37	210.0	10.43	350.0	14.05
325.0	7.74	215.0	10.39	375.0	14.60
350.0	8.08	225.0	10.72	400.0	15.11
375.0	8.41	235.0	11.04	425.0	15.57
400.0	8.70	250.0	11.46	450.0	15.99
425.0	8.99	275.0	12.18	475.0	16.36
450.0	9.24	300.0	12.84		
475.0	9.48	325.0	13.47		

where u is the sound speed, m is mass, $\gamma^0(T) = C_p^0(T)/C_v^0(T)$, and $\beta_a(T)$, $\gamma_a(T)$, and $\delta_a(T)$ are the temperature-dependent acoustic virial coefficients. On each isotherm, $C_p^0(T)$ is obtained from Eq. (2) through the relation $C_p^0(T)/R = \gamma^0/(\gamma^0 - 1)$ and the results are presented in Table I. The $C_p^0(T)/R$ values from Table I along with the CF_4 results of Trusler [1] were fitted with the polynomial:

$$C_P^0(T)/R = A_0 + A_1 T + A_2 T^2 + A_3 T^3 + A_4 T^{-2} \tag{3}$$

The resulting coefficients are presented in Table II.

Figure 2 shows the deviations of the measured values of $C_p^0(T)/R$ from Eq. (3); calculated values of $C_p^0(T)/R$ from the literature are also shown. Nearly all of the data reported here and most of the results from the literature fall within $\pm 0.1\%$ of Eq. (3). In the case of C_2F_6, the highest (460 K) and lowest temperature (210 K) isotherms were omitted from the fit. The 460 K isotherm was determined with only one resonance mode, (3, 0, 0). At this elevated temperature, the other resonances were shifted to high frequencies where the waveguides and horns attenuated the signal drastically. Also, the low vapor densities at the higher temperatures

Table II. Coefficients to Calculate $C_p^0(T)/R$ from Eq. (3)

	A_0	A_1/K	A_2/K^2	A_3/K^3	A_4/K^2
CF_4	-3.48750×10^{-1}	3.55103×10^{-2}	-3.97999×10^{-5}	1.74882×10^{-8}	1.58249×10^{-4}
C_2F_6	5.56480×10^{-1}	5.59322×10^{-2}	-5.78139×10^{-5}	2.10239×10^{-8}	1.30662×10^{-4}

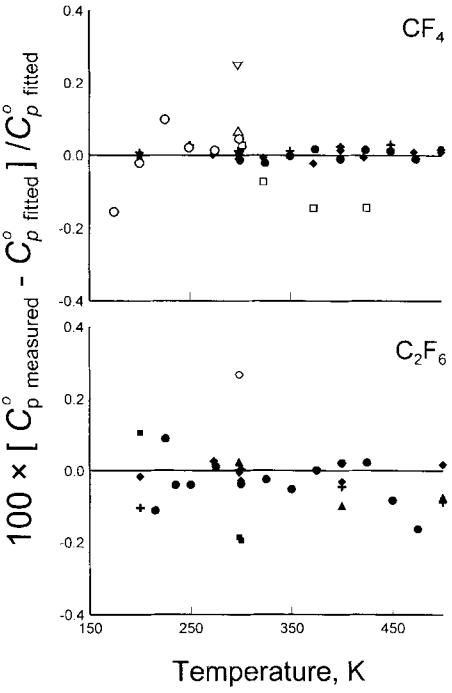

Fig. 2. Percentage deviation of ideal-gas heat capacities, $C_p^0(T)$, from fitted equations. Top: CF_4. Bottom: C_2F_6. (●) is the present work. Published data: (▽) Ref. 20; (■) Ref. 21; (△) Ref. 22; (▲) Ref. 23; (◆) Ref. 24; (+) Ref. 25; (□) Ref. 26; (○) Ref. 1.

contributed to reduced signal strength. These factors reduced the signal-to-noise ratio, while increasing the uncertainty in the measurement of the resonance frequency and half-width. The 210 K isotherm only had three points due to the narrow pressure range available. This introduced greater uncertainty in the extrapolation of Eq. (2) to zero pressure. The fit of Eq. (3) was improved slightly when both of these isotherms were omitted.

After the ideal-gas heat capacities were determined by fitting each isotherm separately, the sound speeds were fitted by the virial equation of state, Eq. (1), with virial coefficients that were smooth functions of temperature. The acoustical virial coefficients in Eq. (2) can be directly related to the density virial coefficients in Eq. (1) through exact thermodynamic equations [10] involving the density virial coefficients, their temperature derivatives, and $\gamma^0(T)$:

$$\beta_a = 2B + 2(\gamma^0 - 1)\, B_t + (\gamma^0 - 1)^2\, B_{tt}/\gamma^0$$

$$\gamma_a = (L - \beta_a B)/(RT) \tag{4}$$

$$\delta_a = (M - \beta_a C - 2RT\gamma_a B)/(RT)^2$$

$$\gamma^0 L = (\gamma^0 - 1)\, Q^2 + (2\gamma^0 + 1)\, C + (\gamma^{02} - 1)\, C_t + (\gamma^0 - 1)^2\, C_{tt}/2 \tag{6}$$

$$\gamma^0 M = (\gamma^0 - 1)^2\, Q^2(2B_t + B_{tt}) + (\gamma^0 - 1)\, QP \tag{5}$$

where $P = 2C + 2\gamma^0 C_t + (\gamma^0 - 1)\, C_{tt}$ and $Q = B + (2\gamma^0 - 1)\, B_t + (\gamma^0 - 1)\, B_{tt}$, and we have introduced the notation $A_t \equiv T(\mathrm{d}A/\mathrm{d}T)$ and $A_{tt} \equiv T^2(\mathrm{d}^2A/\mathrm{d}T^2)$. Equations (4)–(6), relating the acoustical virial coefficients to the density virial coefficients, allow us to fit the virial equation of state to the sound-speed measurements, $u(T, P)$.

Two methods were used to fit the $u(T, P)$ data for both CF_4 and C_2F_6. For the first, the density virial coefficients were expressed as algebraic functions in temperature derived from the hard-core square-well (HCSW) potential model. At each temperature the virial coefficients and their temperature derivatives could be calculated explicitly, allowing a non-linear fit of Eq. (1) to the $u(T, P)$ results. The second, more complicated, method involved fitting the parameters of a more realistic intermolecular potential, the hard-core Lennard–Jones (HCLJ) model. In this case, the density virial coefficients and their derivatives were calculated from integrations over the intermolecular potential. We discuss the results of the HCSW analysis first and then the HCLJ analysis.

5. ANALYSIS

5.1. Analysis with the Hard-Core Square-Well Potential Model (HCSW)

Gillis and Moldover [10] have shown that the equations for the temperature-dependent density virial coefficients derived from the HCSW intermolecular potential model do an excellent job at fitting sound-speed measurements. The HCSW expressions for the virial coefficients have realistic temperature dependences that extrapolate to reasonable values beyond the experimental temperature ranges, and the densities computed from these virial coefficients have small uncertainties in a useful range of conditions [10].

The equations expressing the first two density virial coefficients in terms of the hard-core square-well potential parameters are

$$B(T) = b_0[1 - (\lambda^3 - 1)\Delta] \tag{7}$$

$$C(T) = \tfrac{1}{8}b_0^2(5 - c_1\Delta - c_2\Delta^2 - c_3\Delta^3) \tag{8}$$

$$c_1 = \lambda^6 - 18\lambda^4 + 32\lambda^3 - 15$$

$$c_2 = 2\lambda^6 - 36\lambda^4 + 32\lambda^3 + 18\lambda^2 - 16$$

$$c_3 = 6\lambda^6 - 18\lambda^4 + 18\lambda^2 - 6$$

where $\Delta = e^{\varepsilon/k_B T} - 1$ and k_B is Boltzmann's constant. The adjustable parameters are ε, the well depth; σ, the hard-core diameter; and λ, the ratio of the width of the well to σ. Here b_0 is the molar volume of the hard core, $b_0 = \frac{2}{3}\pi N_A \sigma^3$, where N_A is Avogadro's constant. We follow Ref. 10 in using different values of b_0, ε, and λ for $B(T)$ and for $C(T)$. We determined the density virial coefficients in Eq. (1) from a fit to the measured $u(T, P)$ results using Eqs. (7) and (8) and their temperature derivatives and Eq. (3) to express the acoustic virial coefficients through the relations given by Eqs. (4)–(6) and then substituting the resulting functions into Eq. (2). The best fit parameters are given in Table III.

The fit to the CF_4 data included the measurements of Ewing and Trusler [1], with the exception of their 175 K isotherm. This isotherm would have required terms higher than $C(T)$. For our fitting, the sound speeds measured by Ewing and Trusler on the isotherms 225 and 300 K were multiplied by the factors 1.000065 and 1.000040, respectively, so that their zero pressure sound speeds would be consistent with Eq. (2) and the parameters in Table II. These factors might have resulted from small differences between the purity of the present sample and that of Ewing and Trusler. Figure 3 shows the deviations of the measured sound speeds from those calculated from the HCSW virial equation of state. All of our measured sound speeds are reproduced to within $\pm 0.005\%$. The fit had

Table III. Parameters for HCSW Equations of State Deduced from $u(T, P)$ Measurements

	b_0 ($m^3 \cdot mol^{-1}$)	λ	ε/k_B (K)
	CF_4		
$B(T)$ ($cm^3 \cdot mol^{-1}$)	8.65202×10^{-5}	1.480236	191.8956
$C(T)$ ($cm^3 \cdot mol^{-1}$)^2	8.29090×10^{-5}	1.720815	124.2436
	C_2F_6		
$B(T)$ ($cm^3 \cdot mol^{-1}$)	1.39038×10^{-4}	1.40462	286.2507
$C(T)$ ($cm^3 \cdot mol^{-1}$)^2	1.77713×10^{-4}	1.31904	307.2723
$D(T)$ ($cm^3 \cdot mol^{-1}$)^3	$A_0 = 4.75509 \times 10^{-12}$	$A_1 = -1.51714 \times 10^{-9}$ K	

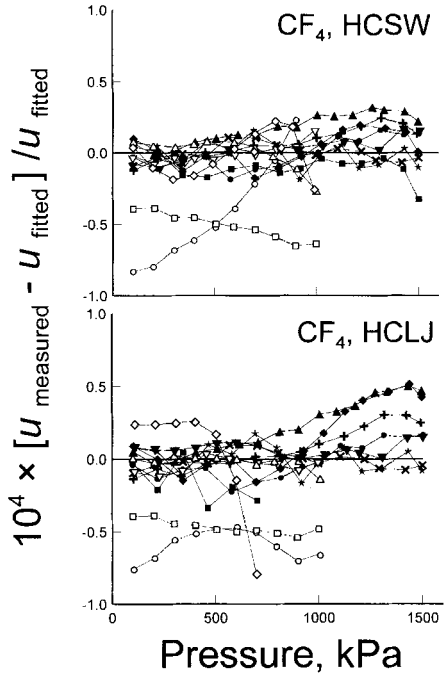

Fig. 3. Deviations of measured sound speeds in CF_4 from the models. Top: Hard-core Square-Well (HCSW). Bottom: Hard-core Lennard–Jones (HCLJ). $\Delta u = u_{meas.} - u_{fit}$. Open symbols from Ref. 1: (◇) 200 K; (○) 225 K; (▽) 250 K; (△) 275 K; (□) 300 K. Filled symbols from this work; (■) 300 K; (◆) 325 K; (▲) 350 K; (+) 375 K; (●) 400 K; (▼) 425 K; (×) 450 K; (★) 475 K.

$v = 158$ degrees of freedom and $\chi^2/v = 0.74$. Figure 2 shows the measurements of Ewing and Trusler before the corrections were applied.

HCSW $B(T)$ and $C(T)$ were fit to the $u(T, P)$ measurements in C_2F_6, but the higher vapor densities required the inclusion of a $D(T)$ term. The $u(T, P)$ measurements did not provide enough detail to fit a square-well representation of $D(T)$; therefore, a two-term polynomial was used, $D(T) = A_0 + A_1 T^{-1}$. The fit had $v = 169$ df and χ^2/v of 1.04. The deviation of the measured $u(T, P)$ from that calculated from the determined equation of state can be seen in Fig. 4. For C_2F_6 almost all measured sound speeds are reproduced to better than 0.005%.

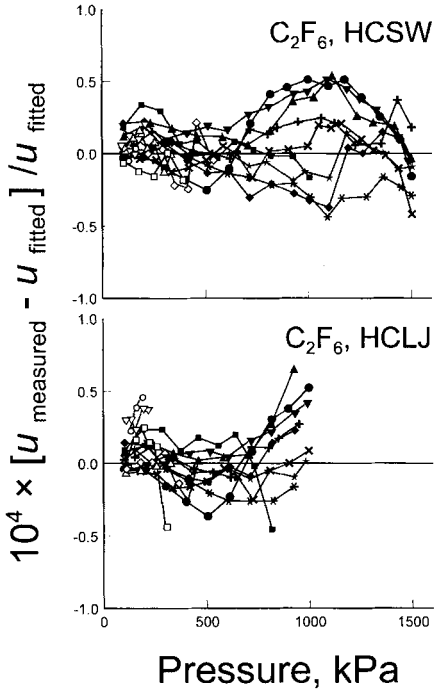

Fig. 4. Deviations of measured sound speeds in C_2F_6 from the models. Top: Hard-core square-well (HCSW). Bottom: Hard-core Lennard–Jones (HCLJ). $\Delta u = u_{meas.} - u_{fit}$. (○) 210 K; (▽) 215 K; (△) 225 K; (□) 235 K; (◇) 250 K; (■) 275 K; (◆) 300 K; (▲) 325 K; (*) 350 K; (●) 375 K; (▼) 400 K; (×) 425 K; (+) 450 K; (★) 475 K.

Figure 5 shows the determined second and third virial coefficients, $B(T)$ and $C(T)$, for CF_4 as represented by Eqs. (7) and (8) and the parameters in Table III. Previously published results are shown for comparison. In almost all cases our virial coefficients reproduce the previously published measurements to within their experimental uncertainties. Also notice that the values calculated from Eqs. (7) and (8) extrapolate reasonably outside of the experimental temperature ranges.

The virial coefficients of C_2F_6 have not been plotted. Pace and Aston [11] measured the second virial coefficient of C_2F_6 in the temperature range 180 K $\leqslant T \leqslant$ 195 K, and Bell et al. [12] report values for $B(T)$ at 280, 300, and 320 K. Our results agree with these measured values to

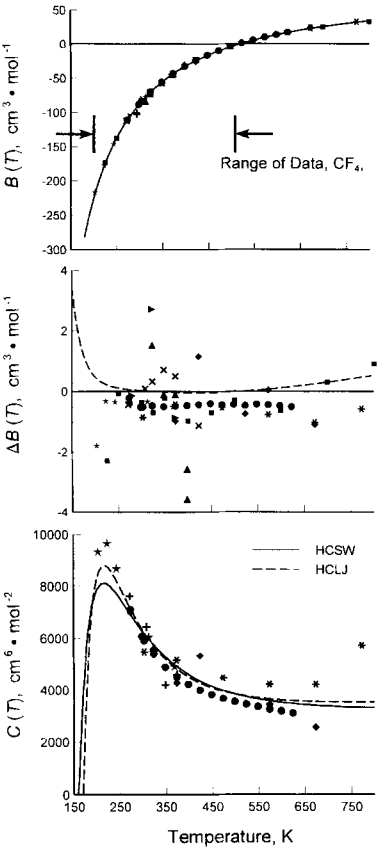

Fig. 5. Virial coefficients of CF_4. Top: The second virial coefficient, $B(T)$. Middle: Differences of $B(T)$ from HCSW ($\Delta B = B_{\text{measured}} - B_{\text{HCSW}}$). Bottom: Third virial coefficient, $C(T)$, for CF_4. (——) Fit to the hard-core Square-Well (HCSW) potential; (– – – –) fit to the hard-core Lennard–Jones (HCLJ) potential. Data: (■) Ref. 27; (+) Ref. 28; (◆) Ref. 29; (▲) Ref. 30; (●) Ref. 31; (∗) Ref. 32; (★) Ref. 33; (×) Ref. 34; (▶) Ref. 35.

within their claimed experimental uncertainties. No previously published third virial coefficients for C_2F_6 could be found in the literature.

5.2. Analysis with the Hard-Core Lennard–Jones (HCLJ) Intermolecular Potential Model

The HCLJ analysis is similar to the HCSW analysis; however, it was more difficult to implement. The hard-core Lennard–Jones potential [2] is

$$\varphi(r_{ij}) = \varepsilon \frac{n}{n-m}\left(\frac{n}{m}\right)^{m/(n-m)} \left\{\left(\frac{\sigma-2a}{r_{ij}-2a}\right)^n - \left(\frac{\sigma-2a}{r_{ij}-2a}\right)^m\right\} \tag{10}$$

where ε is the well depth, σ is the value of r where $\varphi(r)$ crosses zero, a is the radius of the hard core, r_{ij} is the intermolecular separation between molecule i and molecule j, and, in the case of the 6–12 potential, $m = 6$ and $n = 12$. We used the HCLJ potential with the CF_4 and C_2F_6 data in the same way that Trusler used the Maitland–Smith potential with his propane data [13]. (The HCLJ potential worked better than the Maitland–Smith potential with the present data.) For each intermolecular potential, we calculated the classical second and third virial coefficients and their temperature derivatives [14, 15]. The calculation of the third virial coefficient requires inclusion of three-body contributions. Following Trusler [13], we used the Axilrod–Teller triple–dipole term [16]:

$$\varphi(r_{123}) = \frac{\nu_{123}(1+\cos\theta_1\cos\theta_2\cos\theta_3)}{(r_{12}^3 r_{13}^3 r_{23}^3)} \tag{11}$$

where ν_{123} is the dispersion coefficient and θ_i is defined as the angle subtended at molecule i by molecules j and k. This is the first term in the three-body correction to the dispersion energy for monatomic species. The second and third virial coefficients for spherically symmetric molecules are given by

$$B(T) = -2\pi N_A \int_0^\infty f_{12} r_{12}^2 \, dr_{12} \tag{12}$$

$$C(T) = -\frac{8\pi^2 N_A^2}{3} \int_0^\infty \int_0^\infty \int_{|r_{12}-r_{13}|}^{|r_{12}+r_{13}|} (f_{12}f_{13}f_{23} - e_{12}e_{13}e_{23}f_{123}) \times r_{12}r_{13}r_{23} \, dr_{12} \, dr_{13} \, dr_{23} \tag{13}$$

Table IV. Parameters for HCLJ Equations of State Deduced from $u(T, P)$ Measurements

	σ (nm)	ε/k (K)	a (nm)	ν_{123}/k (K · nm^9)
CF_4	0.42982	295.1519	0.073082	0.005745674
C_2F_6	0.50149	423.8087	0.10422	0.025325063

where N_A is Avagadro's number, r_{ij} is the distance between molecule i and molecule j, $e_{ij} = \exp\{-\varphi(r_{ij})/kT\}$, $f_{ij} = e_{ij} - 1$, and $f_{ijk} = \exp\{-\varphi(r_{ijk})/kT\} - 1$. Equations (12) and (13) allow us to calculate the second and third virials for a given intermolecular potential as a function of temperature. With $C_p^0(T)/R$ given by Eq. (3) and the parameters from Table II, only four potential parameters, ε, r_m, a, and ν_{123}, are required to fit the $u(T, P)$ data. Initial guesses of ε, r_m, and a were determined by fitting the HCLJ second virial coefficient to the values determined with the HCSW model. These parameters were fixed, and an initial value for ν_{123} was determined by fitting only ν_{123} to the third virial values determined from the HCSW method. Then all four parameters were varied to fit the $u(T, P)$ measurements. The resulting parameters are given in Table IV.

The computation of the second and third virial coefficients and their temperature derivatives from Eqs. (12) and (13) using the parameters in Table IV is a numerically intensive process and is not convenient for repetitive calculations. Again, following the lead of Trusler [13], we provide a look-up table for the second and third virial coefficients and their first two derivatives, along with a preferred method of interpolation. In the look-up table, a substitution of variables has been performed, such that temperature is presented as a reduced reciprocal temperature, $\tau = \varepsilon/kT$, where $T(dB/dT) = -\tau(dB/d\tau)$, and $T^2(d^2B/dT^2) = \tau^2(d^2B/d\tau^2) + 2\tau(dB/d\tau)$. In Tables V and VI, the virial coefficients are also presented in reduced (unitless) form where $B^*(T) = B(T)/b_0$ and $C^*(T) = C(T)/b_0^2$, where $b_0 = 2\pi N_A\sigma^3/3$. Tables V and VI provide reduced temperatures between 0.3 and 3.0, which correspond to approximately 100 to 1000 K for CF_4 and 140 to 1400 K for C_2F_6. These ranges greatly exceed our experimental temperature ranges; however, they are reasonable extrapolations based on our experience with CF_4 and Trusler's experience with C_3H_8. The recommended interpolation of $B^*(\tau)$, $C^*(\tau)$, or their derivatives at τ between adjacent points at τ_1 and τ_2 is the cubic polynomial $f(\tau)$ such that

$$f(\tau) = a(\tau - \tau_1) + b(\tau - \tau_2) + \{c(\tau - \tau_1) + d(\tau - \tau_2)\}(\tau - \tau_1)(\tau - \tau_2)$$
$$a = f(\tau_2)/\Delta\tau \qquad c = \{f'(\tau_2)/(\Delta\tau)^2\} - \{(a+b)/(\Delta\tau)^2\} \tag{16}$$
$$b = -f(\tau_1)/\Delta\tau \qquad d = \{f'(\tau_1)/(\Delta\tau)^2\} - \{(a+b)/(\Delta\tau)^2\}$$

Table V. CF_4 Reduced Virial Coefficients and Their Derivatives with Respect to Reduced Temperature Deduced from the HCLJ Model

τ	$B(\tau)^*$	$\partial B(\tau)^*/\partial\tau$	$\partial^2 B(\tau)^*/\partial\tau^2$	$\partial^3 B(\tau)^*/\partial\tau^3$	$C(\tau)^*$	$\partial C(\tau)^*/\partial\tau$	$\partial^2 C(\tau)^*/\partial\tau^2$	$\partial^3 C(\tau)^*/\partial\tau^3$
0.3	0.436492	−1.439226	−1.727395	5.443198	0.356237	−0.089809	0.681210	8.852910
0.4	0.284630	−1.592700	−1.401709	1.765508	0.351884	0.012899	1.297572	4.222965
0.5	0.118575	−1.726745	−1.300905	0.440343	0.360261	0.159715	1.603520	2.082608
0.6	−0.060561	−1.855830	−1.290931	−0.173963	0.384530	0.327809	1.732615	0.529964
0.7	−0.252645	−1.986441	−1.327039	−0.520615	0.425999	0.501166	1.708229	−1.053002
0.8	−0.458021	−2.122166	−1.391306	−0.752245	0.484407	0.663703	1.510445	−2.981205
0.9	−0.677328	−2.265371	−1.475758	−0.930966	0.557736	0.795936	1.092290	−5.500800
1.0	−0.911405	−2.417866	−1.576706	−1.085462	0.641746	0.872457	0.382091	−8.867873
1.1	−1.161263	−2.581207	−1.692540	−1.230443	0.729252	0.859342	−0.719611	−13.387340
1.2	−1.428057	−2.756852	−1.822758	−1.374226	0.809127	0.711078	−2.346438	−19.442230
1.3	−1.713091	−2.946243	−1.967519	−1.521986	0.864954	0.366710	−4.675447	−27.523541
1.4	−2.017813	−3.150860	−2.127408	−1.677287	0.873250	−0.255104	−7.939629	−38.265525
1.5	−2.343822	−3.372259	−2.303319	−1.842843	0.801120	−1.262465	−12.444360	−52.489821
1.6	−2.692879	−3.612096	−2.496394	−2.020928	0.603185	−2.798500	−18.588837	−71.261886
1.7	−3.066916	−3.872155	−2.707991	−2.213607	0.217567	−5.052079	−26.893943	−95.963724
1.8	−3.468048	−4.154363	−2.939668	−2.422872	−0.439347	−8.271708	−38.038408	−128.387980
1.9	−3.898596	−4.460816	−3.193185	−2.650734	−1.479737	−12.783562	−52.905697	−170.859810
2.0	−4.361095	−4.793793	−3.470504	−2.899279	−3.053230	−19.014863	−72.644827	−226.394960
2.1	−4.858322	−5.155783	−3.773804	−3.170721	−5.358456	−27.524211	−98.749232	−298.904830
2.2	−5.393309	−5.549500	−4.105491	−3.467430	−8.658073	−39.040918	−133.159060	−393.462640
2.3	−5.969378	−5.977915	−4.468217	−3.791970	−13.298269	−54.516028	−178.393890	−516.649180
2.4	−6.590157	−6.444275	−4.864905	−4.147130	−19.734112	−75.188497	−237.724970	−677.001940
2.5	−7.259616	−6.952135	−5.298765	−4.535949	−28.562437	−102.671050	−315.398780	−885.598820
2.6	−7.982096	−7.505385	−5.773327	−4.961749	−40.564561	−139.061600	−416.927400	−1156.817300
2.7	−8.762347	−8.108286	−6.292468	−5.428168	−56.761713	−187.087840	−549.465650	−1509.322000
2.8	−9.605565	−8.765506	−6.860447	−5.939193	−78.486987	−250.294930	−722.301250	−1967.349600
2.9	−10.517430	−9.482158	−7.481939	−6.499195	−107.478750	−333.289290	−947.492010	−2562.382200

Table VI. C_2F_6 Reduced Virial Coefficients and Their Derivatives with Respect to Reduced Temperature Deduced from the HCLJ Model

τ	$B(\tau)^*$	$\partial B(\tau)^*/\partial\tau$	$\partial^2 B(\tau)^*/\partial\tau^2$	$\partial^3 B(\tau)^*/\partial\tau^3$	$C(\tau)^*$	$\partial C(\tau)^*/\partial\tau$	$\partial^2 C(\tau)^*/\partial\tau^2$	$\partial^3 C(\tau)^*/\partial\tau^3$
0.3	0.519719	−1.204442	−1.520548	4.943202	0.361278	−0.182695	0.375243	8.167618
0.4	0.392306	−1.338975	−1.224003	1.617854	0.346022	−0.112875	0.955612	4.136654
0.5	0.252495	−1.455721	−1.130504	0.423814	0.340117	0.000082	1.275803	2.449345
0.6	0.101313	−1.567727	−1.118708	−0.127448	0.346864	0.138012	1.465107	1.380512
0.7	−0.061090	−1.680815	−1.148173	−0.436938	0.368181	0.289806	1.554410	0.394531
0.8	−0.234994	−1.798188	−1.202710	−0.642523	0.404954	0.445403	1.538351	−0.759330
0.9	−0.420941	−1.921948	−1.275111	−0.800221	0.457002	0.593119	1.391003	−2.259422
1.0	−0.619650	−2.053693	−1.362032	−0.935860	0.522816	0.717807	1.069133	−4.280472
1.1	−0.831991	−2.194788	−1.461995	−1.062660	0.599125	0.799089	0.510843	−7.025144
1.2	−1.058962	−2.346510	−1.574521	−1.188076	0.680276	0.809310	−0.368351	−10.745806
1.3	−1.301689	−2.510115	−1.699719	−1.316732	0.757383	0.710994	−1.681514	−15.765478
1.4	−1.561424	−2.686892	−1.838082	−1.451799	0.817191	0.453598	−3.578535	−22.501935
1.5	−1.839552	−2.878195	−1.990373	−1.595679	0.840565	−0.030694	−6.257029	−31.497595
1.6	−2.137595	−3.085464	−2.157578	−1.750376	0.800504	−0.832423	−9.976632	−43.457610
1.7	−2.457228	−3.310247	−2.340870	−1.917703	0.659530	−2.071951	−15.077626	−59.298970
1.8	−2.800284	−3.554219	−2.541598	−2.099404	0.366263	−3.908682	−22.005156	−80.214064
1.9	−3.168772	−3.819198	−2.761288	−2.297233	−0.149054	−6.553055	−31.340725	−107.753120
2.0	−3.564890	−4.107165	−3.001643	−2.513009	−0.980409	−10.282133	−43.843084	−143.931250
2.1	−3.991043	−4.420278	−3.264552	−2.748661	−2.253645	−15.459873	−60.501380	−191.367490
2.2	−4.449862	−4.760896	−3.552106	−3.006250	−4.136416	−22.563464	−82.604185	−253.465540
2.3	−4.944224	−5.131597	−3.866608	−3.288009	−6.851143	−32.217560	−111.829200	−334.648750
2.4	−5.477278	−5.535201	−4.210594	−3.596361	−10.691889	−45.238767	−150.359830	−440.665810
2.5	−6.052464	−5.974792	−4.586854	−3.933950	−16.046321	−62.693461	−201.036750	−578.988450
2.6	−6.673548	−6.453749	−4.998454	−4.303664	−23.424275	−85.972934	−267.554920	−759.329260
2.7	−7.344649	−6.975772	−5.448763	−4.708665	−33.494925	−116.891080	−354.719950	−994.315950
2.8	−8.070273	−7.544915	−5.941479	−5.152420	−47.135110	−157.811410	−468.781570	−1300.369800
2.9	−8.855350	−8.165617	−6.480665	−5.638730	−65.492196	−211.812190	−617.867710	−1698.850400
3.0	−9.705276	−8.842745	−7.070782	−6.171763	−90.065826	−282.901310	−812.549680	−2217.548800

where $f' = df/d\tau$ and $\Delta\tau = \tau_2 - \tau_1$. To allow the Calculation of second derivatives, third derivatives are included in Tables V and VI. Values calculated with this interpolation method are highly accurate. When comparing values of the virial coefficients and their derivatives calculated directly using Eqs. (12) and (13) to those calculated with the interpolation, it is found that the second virial and its first two derivatives are reproduced to better than 0.01 and 0.05 $cm^3 \cdot mol^{-1}$, respectively, the third virial to better than 1.0 $cm^6 \cdot mol^{-2}$, and its first and second derivatives to better than 2.5 and 15.0 $cm^6 \cdot mol^{-2}$, respectively. The largest errors in the interpolation occur at the lowest temperatures for the third virial where the vapor density is so low that the contribution of the third virial to density is negligible.

For CF_4, the corrected measurements of Ewing and Trusler [1] were incorporated into the HCLJ fit. The ideal-gas heat capacities were fixed at the values given by Eq. (3) and the coefficients in Table II. Figure 3 shows the deviations of the measured sound speeds from the HCLJ analysis. As in the case of the HCSW model, most sound-speed measurements are fitted within $\pm 0.005\%$. The fit had $v = 150$ degrees of freedom and $\chi^2/v = 0.63$, compared to $\chi^2/v = 0.74$ for the HCSW model. Figure 5 compares the second and third virial coefficients determined from the HCLJ model to those determined from the HCSW model. They are remarkably similar.

The measured sound speeds in C_2F_6 were also fitted by the HCLJ model. The data for C_2F_6 at the higher densities required a fourth virial coefficient in the HCSW model. This was also true for the HCLJ model. We chose to exclude data at pressures greater than 1.0 MPa from the fit to avoid fitting the fourth virial coefficient. The calculation of the fourth virial requires a sixfold integration making the nonlinear fitting routine too numerically intensive.

The fit of the HCLJ model to the C_2F_6 data had $v = 112$ degrees of freedom and $\chi^2/v = 1.31$. The HCLJ model does not fit as wide a range of data quite as well as the HCSW model. This is not surprising because the HCLJ model has only four parameters, while the HCSW model has six parameters for $B(T)$ and $C(T)$ and two additional parameters for $D(T)$. Figure 4 shows how the measured sound speeds deviated' from those predicted from the presented equation of state. As in the previous cases, for the most part, the deviations are below 0.005%. The two previous measurements of the second virial coefficient for C_2F_6 discussed earlier are again reproduced.

6. TRANSPORT PROPERTIES

The process of fitting the parameters of the HCLJ intermolecular potential to the $u(T, P)$ results was not a direct attempt at determining the

actual intermolecular potential. The model was only utilized to provide physically correct temperature dependences of the virial coefficients. However, viscosities and thermal conductivities calculated from intermolecular potentials using the kinetic theory of dilute gases [17] demonstrate some predictive ability. Figure 6 compares the vapor viscosities predicted from our HCLJ potential to experimental values from the literature. The baseline is a fit to the published data found in the DIPPR [18] database. The uncertainties of the DIPPR fits are also shown, 3% for CF_4 and 10% for

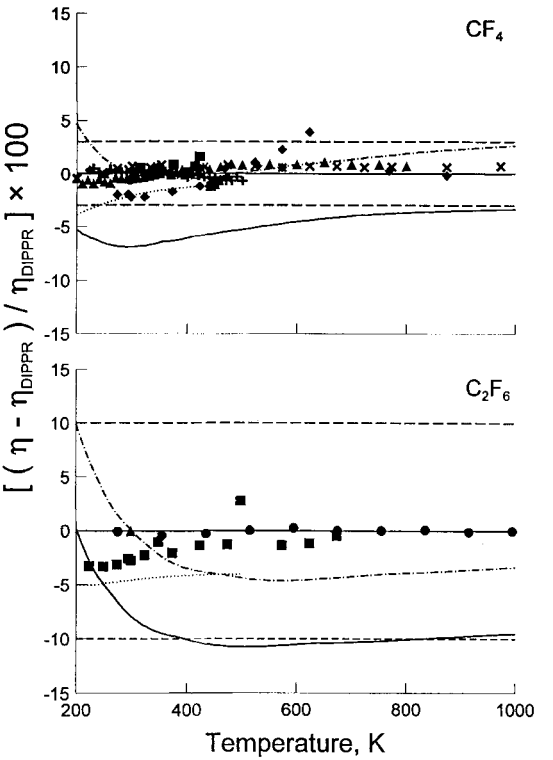

Fig. 6. Deviations of predicted viscosity from the DIPPR [18] database fit to available data $[(\eta_{HCLJ} - \eta_{DIPPR})/\eta_{DIPPR}] \times 100$. (——) Predicted from our HCLJ potential; (– · · ·) predicted from a HCLJ potential fit to both sound speed and viscosity at 300 K; (·····) predicted from a corresponding states model [19]. Top, CF_4: (■) Ref. 36; (+) Ref. 37; (◆) Ref. 38; (▲) Ref. 39; (●) Ref. 40; (*) Ref. 41; (×) Ref. 42; (★) Ref. 43. Bottom, C_2F_6: (■) Ref. 38; (▲) Ref. 44; (●) Ref. 45.

C_2F_6. Figure 6 also show the viscosities predicted from the theory of corresponding states [19] over its limited range of validity. The viscosities predicted from the HCLJ potential are generally within (below) 10% of measured values. The viscosity of propane predicted with Trusler's [13] Maitland–Smith potential (which was deduced from speed-of-sound data) shows similar deviations: +4.2% at 200 K, −1.6% at 300 K, and −6.5% at 500 K.

Based on Fig. 6 and Trusler's results, we suggest that the transport properties deduced from speed-of-sound data will have uncertainties of 10% or less, which might be adequate for engineering purposes. Many of the hazardous, toxic, reactive semiconductor process gases that we plan to investigate fall in this class of compounds.

If a second constraint is available for modeling the intermolecular potential, a better prediction of the transport properties can be made. For example, a HCLJ potential was fit simultaneously to our reported sound speeds in CF_4 and a single viscosity datum of 17.48 μPa · s at 300 K. The resulting parameters were $r_m = 0.408277$ nm, $\varepsilon/k = 365.1938$ K, $a = 0.088944$ nm, and $\nu_{123}/K = 0.004984781$ K · nm^9. The resulting viscosity deviations are shown in Fig. 6. They are generally within the ±3% uncertainty of the DIPPR fit from 200 to 1000 K.

The HCLJ is not the correct representation of the true intermolecular potential, having only three adjustable parameters (four counting the three-body contribution). Thus, it is not surprising that the simultaneous fit does not represent the sound-speed measurements to within their uncertainties. The simultaneous fit reproduced the sound-speed measurements only to within ±0.07%, in comparison with ±0.005% when only the sound speeds are fitted. However, over the temperature and pressure ranges of our sound-speed measurements, the predicted densities of the simultaneous fit differ from our recommended equation of state by an average of only 0.019% with a maximum deviation of 0.076% at 200 K and 500 kPa, the highest density state. Perhaps a fit using a more flexible potential model with more parameters would yield superior results.

7. DISCUSSION AND CONCLUSION

Sound-speed measurements in CF_4 and C_2F_6 have been presented. The CF_4 measurements cover the temperature range 300 to 475 K, while the C_2F_6 measurements range from 210 to 475 K. In both cases the pressure range examined was 0.1 to 1.5 MPa, or 80% of the samples' vapor pressure, whichever was lower.

The sound speeds were collected along isotherms, and from the zero-pressure intercept of each isotherm, the ideal-gas heat-capacity $C_p^0(T)$ was

determined. The measured values of $C_p^0(T)$ correspond well with values calculated from statistical thermodynamics and spectroscopic measurements. Two methods of data reduction were employed to deduce the virial equation of state for each of the gases: the hard-core square-well model and the hard-core 6–12 Lennard–Jones model. The second and third virial coefficients determined from the two methods nearly agree. The differences in calculated vapor densities from the two equations of state are well below 0.1 %, our estimated uncertainty. The temperature dependences of the virial coefficients derived from the HCLJ model are more accurate; however, the results are presented in a look-up table that may be less convenient to employ. The simple algebraic expressions derived for the HCSW model nearly agree with the more physically accurate HCLJ model, even outside the experimental temperature range.

We have shown that from measured sound speeds in the vapor phase, we can obtain ideal-gas heat capacities accurate to 0.1 % and generate an equation of state capable of predicting vapor densities to within 0.1 %. The equation of state is based on a physical model, which can be extrapolated with confidence to temperatures outside our experimental range. The HCLJ equation of state should be valid from the triple point to in excess of 1000 K at low to moderate pressures. We have also shown that for compounds for which no measurements of transport properties have been made, our fitting of a realistic intermolecular potential to the sound speeds can predict transport properties to within 10 % over wide ranges, providing needed property estimates in cases where none had, previously existed.

APPENDIX

Table AI. Measured Sound Speeds in CF_4

P (kPa)	u ($m \cdot s^{-1}$)	$\sigma[u]/u$ ($\times 10^6$)
	$T = 300.00$ K	
1500.01	175.080	46.4
1427.51	175.361	49.6
1330.27	175.737	51.3
1223.45	176.151	41.8
1127.03	176.529	46.0
1025.55	176.928	34.0
923.26	177.333	16.6
822.19	177.735	15.7
703.64	178.210	20.6
583.00	178.695	17.6

Table AI. *(Continued)*

P (kPa)	u ($m \cdot s^{-1}$)	$\sigma[u]/u$ ($\times 10^6$)
464.29	179.176	13.8
343.19	179.671	10.3
221.26	180.173	20.0
99.89	180.673	20.0
	$T = 325.00$ K	
1499.18	183.469	60.7
1439.87	183.630	60.7
1339.70	183.900	54.8
1214.89	184.241	42.0
1129.53	184.477	37.2
1023.71	184.770	29.6
927.85	185.039	26.3
815.33	185.358	15.4
698.18	185.695	17.9
584.35	186.029	2.6
460.14	186.395	4.5
342.10	186.744	54.8
219.10	187.116	
102.21	187.472	
	$T = 350.00$ K	
1498.43	191.227	56.6
1434.34	191.344	52.9
1333.32	191.531	46.8
1275.66	191.639	40.9
1178.81	191.821	36.7
1088.33	191.994	28.7
1004.84	192.157	24.3
903.23	192.356	20.6
812.32	192.537	16.1
706.90	192.750	15.1
616.10	192.936	7.4
509.21	193.158	10.6
405.48	193.377	6.0
304.57	193.591	2.5
203.63	193.809	
101.89	194.032	
	$T = 375.00$ K	
1492.54	198.503	45.4
1424.37	198.584	37.3

Table AI. *(Continued)*

P (kPa)	u ($m \cdot s^{-1}$)	$\sigma[u]/u$ ($\times 10^6$)
1317.97	198.711	34.8
1220.02	198.830	30.9
1122.29	198.951	27.2
1001.24	199.105	15.9
911.49	199.222	15.4
812.45	199.352	20.4
694.00	199.514	5.8
571.32	199.684	16.4
455.27	199.850	—
334.61	200.024	—
219.05	200.196	—
103.22	200.370	
203.63	193.791	
101.89	194.015	—
	$T = 400.00$ K	
1503.46	205.387	29.3
1429.79	205.435	29.8
1315.31	205.513	25.4
1210.60	205.585	23.6
1105.52	205.662	16.8
1010.02	205.733	15.5
922.75	205.800	16.1
816.97	205.883	18.2
700.84	205.979	6.6
579.61	206.082	0.8
453.00	206.197	6.2
340.72	206.300	5.1
219.06	206.413	41.3
99.99	206.531	33.2
	$T = 425.00$ K	
1502.98	211.966	99.6
1425.12	211.984	92.3
1305.13	212.014	86.4
1195.12	212.046	84.0
1133.07	212.066	75.3
1029.58	212.099	77.0
904.89	212.142	63.5

Table AI. *(Continued)*

P (kPa)	u ($m \cdot s^{-1}$)	$\sigma[u]/u$ ($\times 10^6$)
822.73	212.173	68.1
699.30	212.222	67.6
573.21	212.276	62.1
457.07	212.329	67.7
338.41	212.383	81.1
220.35	212.441	3.3
101.11	212.505	—
	$T = 450.00$ K	
1501.53	218.263	32.6
1419.58	218.255	33.8
1292.89	218.247	20.6
1222.44	218.244	29.0
1104.48	218.241	25.3
998.24	218.239	11.0
922.83	218.240	11.7
805.60	218.244	14.0
702.14	218.250	10.3
568.86	218.260	9.7
462.96	218.267	4.6
342.96	218.281	44.6
222.59	218.297	66.3
101.21	218.316	86.8
	$T = 475.00$ K	
1499.90	224.339	—
1432.20	224.316	—
1307.92	224.271	—
1210.93	224.238	—
1123.55	224.214	—
1020.95	224.183	—
918.63	224.149	—
797.00	224.121	—
692.17	224.100	—
579.22	224.071	—
465.96	224.050	—
339.63	224.021	—
217.34	224.004	—
109.32	223.990	—

Table AII. Measured Sound Speeds in C_2F_6

P (kPa)	u ($m \cdot s^{-1}$)	$\sigma[u]/u$ ($\times 10^6$)
	$T = 210.00$ K	
182.35	112.218	53.5
155.24	113.212	48.7
125.55	114.267	84.9
	$T = 215.00$ K	
211.53	112.926	31.4
188.73	113.724	46.9
152.53	114.952	42.8
132.21	115.624	41.8
102.10	116.599	32.1
	$T = 225.00$ K	
334.16	112.463	37.1
298.59	113.638	27.8
247.87	115.255	7.1
214.82	116.269	21.6
181.92	117.254	40.7
145.70	118.307	92.8
105.77	119.433	63.1
	$T = 235.00$ K	
390.25	114.639	21.4
318.18	116.718	3.0
247.01	118.666	2.5
175.65	120.528	24.0
102.20	122.361	101.4
102.20	122.362	120.5
	$T = 250.00$ K	
529.24	116.767	29.2
460.42	118.477	19.5
410.54	119.667	1.1
351.57	121.041	28.9
287.16	122.494	5.1
224.65	123.859	14.7
162.19	125.183	47.3
101.61	126.432	97.3
	$T = 275.00$ K	
1004.88	116.731	17.0
925.01	118.373	12.2
816.86	120.512	11.5

Table AII. *(Continued)*

P (kPa)	u ($m \cdot s^{-1}$)	$\sigma[u]/u$ ($\times 10^6$)
732.48	122.121	1.0
639.97	123.827	4.8
556.80	125.315	13.0
459.32	127.008	8.0
374.43	128.440	31.9
284.07	129.927	59.9
190.35	131.426	51.7
103.23	132.782	10.0
103.23	132.792	10.0
	$T = 300.00$ K	
1495.54	119.856	2.3
1438.85	120.742	3.5
1361.38	121.933	5.9
1265.85	123.369	11.3
1193.60	124.436	23.9
1099.40	125.797	11.7
1005.89	127.125	33.9
930.28	128.181	35.7
821.26	129.674	20.0
714.55	131.102	32.4
613.53	132.431	33.0
509.00	133.778	4.9
412.56	134.999	3.2
306.06	136.323	12.7
205.26	137.556	43.1
103.04	138.782	7.8
	$T = 325.00$ K	
1501.11	130.574	12.2
1420.72	131.423	19.1
1316.62	132.515	31.6
1238.54	133.327	20.3
1116.70	134.584	24.8
1027.75	135.488	23.4
926.73	136.508	8.0
816.33	137.608	30.7
706.53	138.694	12.4
583.26	139.901	25.4
460.36	141.091	34.1
338.63	142.256	57.9
234.58	143.242	53.3
104.42	144.461	12.4

Table AII. *(Continued)*

P (kPa)	u ($m \cdot s^{-1}$)	$\sigma[u]/u$ ($\times 10^6$)
	$T = 350.00$ K	
1501.27	139.426	88.8
1451.42	139.805	83.9
1364.43	140.466	39.7
1282.98	141.081	33.9
1164.23	141.980	46.6
1094.54	142.505	19.7
1009.88	143.147	7.9
925.78	143.782	5.5
823.79	144.550	22.1
711.25	145.395	30.4
607.23	146.174	29.3
515.93	146.856	38.3
411.69	147.632	43.3
303.07	148.438	62.8
206.62	149.153	73.9
100.49	149.931	—
	$T = 375.00$ K	
1501.34	147.110	34.3
1446.80	147.419	28.2
1350.92	147.960	26.1
1261.42	148.468	33.7
1177.49	148.946	43.7
1099.32	149.390	61.1
999.67	149.961	57.8
898.62	150.538	72.9
816.92	151.008	62.0
720.36	151.562	47.0
614.67	152.167	9.8
505.89	152.794	10.1
403.18	153.390	8.0
303.70	153.968	10.2
202.37	144.557	33.8
101.53	145.143	58.5
	$T = 400.00$ K	
1503.31	153.996	24.3
1444.16	154.247	28.3
1339.22	154.691	26.9
1242.42	155.105	27.4
1192.95	155.318	28.2
1095.71	155.738	37.7

Table AII. *(Continued)*

P (kPa)	u ($m \cdot s^{-1}$)	$\sigma[u]/u$ ($\times 10^6$)
991.50	156.190	37.3
928.14	156.467	30.5
812.66	156.975	28.6
711.65	157.422	36.1
602.21	157.909	53.3
507.22	158.336	65.6
412.04	158.765	67.5
304.93	159.250	81.2
204.44	159.707	79.3
100.25	160.181	20.0
	$T = 425.00$ K	
1503.68	160.312	6.6
1438.88	160.805	3.1
1376.24	160.466	1.2
1316.95	160.081	3.0
1260.07	161.980	10.0
1162.47	161.505	13.4
1112.56	161.147	22.2
1053.37	161.782	25.9
997.44	161.550	20.1
903.24	162.395	29.5
810.29	162.174	31.8
727.08	162.856	14.0
652.67	163.632	41.7
586.07	163.438	43.9
504.46	163.153	46.4
420.21	163.931	44.2
335.61	164.210	54.7
260.88	164.476	57.7
181.24	164.760	55.7
103.06	165.040	17.5
	$T = 450.00$ K	
1503.93	166.204	13.2
1435.11	166.363	21.0
1353.92	166.546	13.4
1228.88	166.841	15.2
1128.66	167.084	1.1
1065.72	167.238	6.6
951.37	167.521	12.5
849.86	167.776	19.1
802.88	167.895	26.1

Table AII. *(Continued)*

P (kPa)	u ($m \cdot s^{-1}$)	$\sigma[u]/u$ ($\times 10^6$)
718.02	168.113	33.9
618.71	168.369	29.3
533.15	168.595	42.5
440.05	168.844	51.0
337.43	169.122	60.1
243.93	169.378	61.2
152.89	169.627	44.6
	$T = 475.00$ K	
1505.03	171.728	27.9
1432.87	171.844	10.0
1363.97	171.959	24.3
1246.46	172.158	33.7
1187.75	172.259	32.0
1102.60	172.403	10.6
983.55	172.617	14.4
927.37	172.718	11.4
797.49	172.961	24.3
712.76	173.122	27.1
614.42	173.313	43.3
529.38	173.479	45.4
433.48	173.671	59.1
347.62	173.846	62.0
242.97	174.060	48.3
151.22	174.253	65.5

REFERENCES

1. M. B. Ewing and J. P. M. Trusler, *J. Chem. Phys.* **90**:1106 (1989).
2. T. Kihara, *Rev. Mod. Phys.* **25**:831(1953).
3. A. R. H. Goodwin and M. R. Moldover, *J. Chem. Phys.* **95**:5236 (1991).
4. K. A. Gillis, *Int. J. Thermophys.* **18**:73 (1997).
5. K. A. Gillis, *Int. J. Thermophys.* **15**:821 (1994).
6. K. A. Gillis, A. R. H. Goodwin, and M. R. Moldover, *Rev. Sci. Instrum.* **62**:2213 (1991).
7. International Fire Code Institute, *Uniform Fire Code*, 1994 ed.
8. American Society of Mechanical Engineers. Boiler and Pressure Vessel Committee, *Qualification Standard for Welding Procedures, Welders, and Welding Operators*, 1998 ed.
9. J. W. S. Rayleigh, *Theory of Sound* (Dover, New York, 1945).
10. K. A. Gillis and M. R. Moldover, *Int. J. Thermophys.* **17**:1305 (1996).
11. E. L. Pace and J. G. Aston, *J. Am. Chem. Soc.* **70**:566 (1948).
12. T. N. Bell, C. M. Bignell, and P. J. Dunlop, *Physica A* **181**:221 (1992).
13. J. P. M. Trusler, *Int. J. Thermophys.* **18**:635 (1997).
14. E. A. Mason and T. H. Spurting, *The Virial Equation of State* (Pergamon, Oxford, 1969).

15. R. J. Dulla, J. S. Rowlinson, and W. R. Smith, *Mol. Phys.* **21**:229 (1971).
16. B. M. Axilrod and E. J. Teller, *J. Chem. Phys.* **11**:299 (1943).
17. J. O. Hirschfelder, C. F. Curtiss, and R. B. Bird, *Molecular Theory of Gases and Liquids* (Wiley, New York, 1954).
18. BYU DIPPR801 Thermophysical Properties Database (Brigham Young University, Provo, UT, 1998).
19. S. A. Klein, M. O. McLinden, and A. Laesecke, *Int. J. Refrig.* **20**:208 (1997).
20. Landolt-Bornstein, *Zahlenwerte und Funktionen, Vol. 2, Part 4. Kalorische Zustandsgrossen*, 6th ed. (Springer-Verlag, Berlin, 1961).
21. L. V. Gurivich, *Thermodynamic Properties of Chemical Substances, Vol. 2* (Academy of Sciences, USSR, 1962).
22. D. D. Wagman, W. H. Evans, V. B. Parker, I. L. Halow, S. M. Bailey, and R. H. Schumm, *Selected Values of chemical Thermodynamic Properties*, National Bureau of Standards Technical Note 270-3 (1968).
23. D. R. Stull, E. F. Westrum, and G. C. Sinke, *The Chemical Thermodynamics of Organic Compounds* (Wiley, New York, 1969).
24. A. S. Rodgers, J. Chao, R. C. Wilhoit, and B. J. Zwolinski, *J. Phys. Chem. Ref. Data* **3**:117 (1974).
25. M. W Chase, C. A. Davies, J. R. Downey, D. J. Frurip, R. A. McDonald, and A. N. Syverud, *J. Phys. Chem. Ref. Data (Suppl. 1)* **14**:1 (1985).
26. Y. T. Hwang and H. H. Martin, *AIChE J.* **10**:89 (1964).
27. J. H. Dymond and E. B. Smith, *The Virial Coefficients of Pure Gases and Mixtures* (Oxford Press, New York, 1980).
28. W. Cawood and H. S. Patterson, *Phil. Trans. Roy. Soc.* **A236**:77 (1937).
29. K. E. MacCormack and W. G. Schneider, *J. Chem. Phys.* **19**:845 (1959).
30. S. D. Hamann, J. A. Lambert, and W. J. McManamey, *Aust. J. Chem.* **7**:1 (1954).
31. D. R. Douslin, R. H. Harrison, R. T. Moore, and J. P. McCullough, *J. Chem. Phys.* **35**:1357 (1961).
32. N. K. Kalfoglou and J. G. Miller, *J. Phys. Chem.* **71**:1256 (1967).
33. H. B. Lange and F. P. Stein, *J. Chem. Eng. Data* **15**:56 (1970).
34. P. M. Sigmund, I. H. Silberberg, and J. J. McKetta, *J. Chem. Eng. Data* **17**:168 (1972).
35. T. K. Bose, J. S. Sochanski, and R. H. Cole, *J. Chem. Phys.* **57**:3592 (1972).
36. J. Timmermans, *Physico-Chemical Constants of Pure Organic Substances*, 2nd ed. (Elsevier, New York, 1965).
37. Y. S. Touloukian, *Thermophysical Properties of Matter* (IFI/Plenum, New York, 1970).
38. W. Braker and A. L. Mossman, *Matheson Gas Data Book*, unabridged ed. (Matheson, East Rutherford, NJ, 1974).
39. J. M. Hellemans, *Physica* **65**:276 (1973).
40. R. M. Young, W. R. F. Vale, J. Scrivins, A. M. Robinson, M. W. Pailthorpe, J. D. Lambert, and K. J. Cotton, *Proc. Roy. Soc. (London) A* **231**:280 (1955).
41. N. M. Singh and J. C. McCoubrey, *Trans. Faraday Soc.* **53**:877 (1957).
42. W. A. Wakeham, S. T. Ro, and J. Kestin, *Trans. Faraday Soc.* **67**:2308 (1971).
43. E. A. Mason, J. Kestin, J. Bzowski, and A. Bousheri, *J. Phys. Chem. Ref. Data* **16**:445 (1987).
44. Freon Products (E. I. DuPont de Nemours, Freon Products Division, Wilmington, DE, 1969).
45. D. Reichenberg, *The Viscosity of Organic Vapors at Low Pressures*, DSC Rep. 11 (National Physical Laboratory, Teddington, England, 1971).